- 1 **Title:** The Alaska Amphibious Community Seismic Experiment
- 2
- 3 Authors: Grace Barcheck^{1*}, Geoffrey A. Abers¹, Aubreya N. Adams², Anne Bécel³, John Collins⁴,
- 4 James B. Gaherty⁵, Peter J. Haeussler⁶, Zongshan Li⁷, Ginevra Moore⁸, Evans Onyango⁹, Emily
- 5 Roland⁸, Daniel E. Sampson¹⁰, Susan Y. Schwartz¹⁰, Anne F. Sheehan¹¹, Donna J. Shillington⁵,
- 6 Patrick J. Shore⁷, Spahr Webb³, Douglas A. Wiens⁷, Lindsay L. Worthington⁹
- 7
- 8 *Corresponding Author:
- 9 Grace Barcheck, grace.barcheck@cornell.edu
- 10 Department of Earth and Atmospheric Sciences, Cornell University, 112 Hollister Drive, Ithaca,
- 11 NY, 14853-1504, USA.
- 12
- 13 **Affiliations:**
- 14 ¹ Department of Earth and Atmospheric Sciences, Cornell University, 112 Hollister Drive, Ithaca,
- 15 NY, 14853-1504, USA.
- ² Department of Geology, Colgate University, 13 Oak Drive, Hamilton, NY, 13346, USA.
- 17 ³ Lamont-Doherty Earth Observatory, Columbia University, P.O. Box 1000, 61 Route 9W,
- 18 Palisades, NY 10964
- 19 ⁴ Department of Geology and Geophysics, Woods Hole Oceanographic Institution, Mail Stop:
- 20 24, 266 Woods Hole Rd., Woods Hole, MA, 02543-1050, USA
- ⁵ School of Earth and Sustainability, Northern Arizona University, Room A108 Building 11,
- 22 Ashurst, 624 S Knoles Dr., Flagstaff, AZ, 86011, USA

- ⁶ U.S. Geological Survey, Alaska Science Center, 4210 University Dr., Anchorage, AK, 99508, USA
- ⁷ Department of Earth and Planetary Sciences, Washington University in St. Louis, Campus Box
- 25 1169, 1 Brookings Dr., St. Louis, MO, 63130-4899, USA
- ⁸ School of Oceanography, University of Washington, 1503 NE Boat St., Box 357940, Seattle,
- 27 WA, 98195-7940, USA
- ⁹ Department of Earth and Planetary Sciences, University of New Mexico, 1 University Place,
- 29 Albuquerque, NM, 87131-0001, USA
- 30 ¹⁰ Department of Earth and Planetary Sciences, University of California Santa Cruz, 1156 High
- 31 Street, Santa Cruz, CA 95064
- 32 ¹¹ Cooperative Institute for Research in Environmental Sciences and Department of Geological
- 33 Sciences, University of Colorado, Boulder, Colorado 80309, USA

35 **Abstract:**

34

36 The Alaska Amphibious Community Seismic Experiment (AACSE) is a shoreline-crossing passive-37 and active-source seismic experiment that took place from May 2018 through August 2019 38 along a ~700 km long section of the Aleutian subduction zone spanning Kodiak Island and the 39 Alaska Peninsula. The experiment featured 105 broadband seismometers, 30 deployed onshore 40 and 75 deployed offshore in Ocean Bottom Seismometer (OBS) packages. Additional strong 41 motion instruments were also deployed at six onshore seismic sites. Offshore OBS stretched 42 from the outer rise across the trench to the shelf. OBS in shallow water (< 300 m depth) were 43 deployed with a trawl-resistant shield, and deeper OBS were unshielded. Additionally, a 44 number of OBS-mounted strong motion instruments, differential and absolute pressure gauges, hydrophones, and temperature and salinity sensors were deployed. OBS were deployed on two cruises of the R/V *Sikuliaq* in May and July 2018 and retrieved on two cruises aboard the R/V *Sikuliaq* and R/V *Langseth* in August-September 2019. A complementary 398–instrument nodal seismometer array was deployed on Kodiak Island for 4 weeks in May-June 2019, and an active source seismic survey on the R/V *Langseth* was arranged in June 2019 to shoot into the AACSE broadband network and the nodes. Additional underway data from cruises include seafloor bathymetry and sub-bottom profiles, with extra data collected near the rupture zone of the 2018 M7.9 offshore-Kodiak earthquake. The AACSE network was deployed simultaneously with the EarthScope Transportable Array (TA) in Alaska, effectively densifying and extending the TA offshore in the region of the Alaska Peninsula. AACSE is a community experiment, and all data were made available publicly as soon as feasible in appropriate repositories.

1. Introduction

The Alaska-Aleutian megathrust offshore of the Alaska Peninsula is an excellent locale to study the inner workings of a subduction zone. The region between Kodiak Island and Sanak Island (Figure 1) features first-order along-strike variation in seismicity, coupling, and incoming plate structure and hydration complemented by systematic variation in arc magmatic chemistry (Davies et al., 1981; von Huene et al., 2012; Buurman et al., 2014; Shillington et al., 2015; Li and Freymueller, 2018). The rupture extent of the second largest earthquake ever recorded, the 1964 M9.2 Great Alaska Earthquake, extends along the megathrust beneath Kodiak Island, and several additional historical megathrust ruptures occurred in the region (Figure 1). In 1938, a M8.3 earthquake occurred on the now-locked Semidi segment southwest of Kodiak Island

(Estabrook et al., 1994), and in 1946, a large tsunami-generating earthquake occurred near Sanak Island, with magnitude estimates ranging from M7.4 to M8.6 (Johnson and Satake, 1997; Lopez and Okal, 2006). Yet the megathrust interface near the Shumagin Islands between these two historical events has not ruptured in at least the last 170 years (Davies et al., 1981), and possibly for most of Holocene time (Witter et al., 2014). GPS evidence suggests low-to-no coupling, with aseismic creep occurring in the Shumagin segment (Li and Freymueller, 2018). Background seismicity rate varies substantially along strike as well, with higher rates in the creeping Shumagin segment, and lower in the Semidi segment (Shillington et al., 2015). The complex M7.9 January 2018 offshore Kodiak earthquake (Ruppert et al., 2018) also occurred at the eastern edge of this region. Finally, this volcanic arc segment shows noteworthy behavior and variation. This segment has hosted numerous Holocene caldera-forming eruptions, including the largest 20th century eruption at Katmai. It also shows along-strike compositional variations linked with the transition from a continental to more oceanic upper plate (e.g., Buurman et al., 2014; Miller & Smith, 1987).

The Alaska Amphibious Community Seismic Experiment (AACSE) was designed to leverage onshore-offshore instrumentation that crosses this along-strike variability to test hypotheses related to seismic slip, subduction zone structure, and arc magmatic compositions (Abers et al., 2019). This shoreline-crossing geophysical experiment (Figure 1) includes seismic instrumentation deployed from May 2018 through September 2019 in a study region ~700 km along-strike and ~500 km perpendicular to the Aleutian trench. Data were recorded

contemporaneously with the EarthScope Transportable Array (TA) in Alaska, effectively densifying and extending the TA offshore near the Alaska Peninsula.

The core of the AACSE dataset comes from an array of 75 broadband ocean bottom seismometers (OBS) and 30 broadband land seismometers operated for 13-16 months in 2018-2019 (Figure 1; Supplementary Table S1). These are complemented by a range of additional geophysical data from other instrumentation and sources: strong-motion seismic instruments, ocean-bottom differential and absolute pressure gauges, hydrophones, ocean-bottom temperature and salinity sensors, a temporary array of 398 nodal seismometers on Kodiak Island, and an active-source seismic experiment.

AACSE is a 'community' experiment (Abers et al., 2019). The project was designed through open community forums and workshops, beginning with a 2014 workshop on the future of amphibious seismology. The AACSE proposal was written in response to the March 2016 Dear Colleague Letter from NSF (DCL 16-061) that requested community-based proposals for a large amphibious seismic array located in the GeoPRISMS and EarthScope focus area of the Alaska-Aleutian subduction zone. The ten-member PI team was created following an open application process. The experiment was coordinated by the PI team, and supported by operators of the IRIS-PASSCAL Instrument Center, the Woods Hole and Lamont-Doherty Ocean Bottom Seismometer Instrument Pool operators, the University of Utah nodal pool, operators of oceanographic research vessels R/V Sikuliaq (University of Alaska Fairbanks) and R/V Marcus G. Langseth (Lamont-Doherty Earth Observatory), the Alaska Volcano Observatory (AVO), the

Alaska Earthquake Center (AEC), and numerous local agencies, land owners and vessel operators. As a community experiment, all data were made publicly available through appropriate repositories as soon as metadata generation and standard corrections could be done (see Data and Resources section, Table S2).

This article outlines the motivation for the AACSE project, the datasets collected onshore and offshore, a description of seismic noise characteristics across the network, known issues with the data, and several data examples. The intent is to provide an overview of data availability and highlight nonstandard aspects of the data that may be of interest to potential users.

2. Instrument Deployment Details

2.1. Passive source broadband seismic network and related data streams

The AACSE project leverages a wide variety of geophysical data (Table S2). The full network of 105 seismometers (Figure 1) was operational approximately July 2018 through August 2019. Figure 2 contains a record section of the Nov. 2018 M7.1 Anchorage earthquake as recorded by AACSE stations, showing high quality data recorded across the network by both land and ocean bottom sensors. Data from the integrated onshore-offshore seismic network is available under network code "XO" via the IRIS Data Management Center (IRIS DMC) (dmc.iris.edu). All instrumentation and channel codes are reported in Table S2.

Onshore, 30 Nanometrics Trillium 120PHQ broadband seismometers from the IRIS-PASSCAL Instrument Center were operated across the study area from May 2018 through Sept. 2019. At

six sites, these were accompanied by Nanometrics Titan accelerometers (onshore red circles, Figure 1). Land station codes are variable but designated largely by geographic location, discussed in the Supplement. Broadband seismometers and accelerometers recorded data at both 100 and 1 Hz on Quanterra Q330 data loggers. Land instruments were deployed in May-June 2018, a subset were serviced Aug. 23 through Sept. 7, 2018 and May 16 through 24, 2019, and all were recovered in Aug. 2019. Servicing involved refurbishing damaged stations and retrieving data. The systems were powered by one or two 18–V arrays of air-alkaline batteries, capable of running a station for the duration of the experiment without charging or replacement. To resist bear damage (e.g., Tape et al., 2019), effort went into designing hard aluminum boxes to protect instrumentation and batteries. Nevertheless, some stations on Kodiak Island suffered data degradation or loss following bear visits, principally through the loss of the GPS clock antenna. Details of known data degradation and timing errors are reported in Table S1.

Offshore, 75 OBS packages provided from the Ocean Bottom Seismograph Instrument Pool (OBSIP) were deployed during two cruises on the R/V *Sikuliaq* (cruise numbers SKQ201811S and SKQ201816S). The Lamont Doherty Earth Observatory (LDEO) supplied 45 OBS packages, deployed in May 2018. All LDEO OBS included a Nanometrics Trillium Compact broadband seismometer. Twenty were designed for shallow water deployment and have a protective trawl-resistant shield (trawl-resistant mounted, or TRM). These were built for the Cascadia Initiative (Toomey et al., 2014) and have station codes LT## (where ## represents a range of numerical station codes). All of the shallow-water instruments also include an absolute

pressure gauge (APG) and a hydrophone. These shielded OBS did not include floatation and were recovered by either pop-up buoy or using the Remotely Operated Vehicle (ROV) *Jason*. The remaining 25 LDEO OBS were deployed in deep water: 10 with a differential pressure gauge (DPG) (station codes LD##), and 15 with an APG and a hydrophone (station codes LA##). All APGs operated on a data logging system independent from other sensors, and APG data include an ocean temperature data stream (channel code HKO). Broadband seismometers, DPGs, and hydrophones recorded at 100 Hz, and APGs recorded at 125 Hz. LDEO OBS were deployed for roughly 15 months.

The Woods Hole Oceanographic Institution (WHOI) provided 30 OBS packages, deployed in July 2018. All of these broadband OBS packages contained a Guralp CMG 3T broadband seismometer and a Scripps Institution of Oceanography Differential Pressure Gauge (DPG), and 5 OBS packages contained an additional Kinemetrics Episensor accelerometer (offshore red circles, Figure 1). Broadband-only WHOI OBS have station codes WD##, whereas sites with accelerometers have station codes WS71-WS75. WHOI broadband seismometers, accelerometers, and most DPGs recorded at both 100 and 1 Hz. DPGs on packages with accelerometers recorded at 40 and 1 Hz. WHOI OBS were deployed for roughly 13 months. An example local earthquake recorded on a seven-component WHOI OBS is shown in Figure 3.

The LDEO OBS were recovered using the R/V *Sikuliaq* in August 2019 (cruise SKQ201918S), and WHOI OBS were recovered using R/V *Marcus G. Langseth* in August-September 2019 (cruise MGL1907).

AACSE was intentionally deployed while the EarthScope TA was at full deployment in Alaska. Consequently, all TA seismic data can be used as part of any AACSE-based study, as well as open seismic data from the Alaska Volcano Observatory, the Alaska Earthquake Center, the Alaska Tsunami Warning Center, and other local agencies (Figure 1).

2.2. Additional geophysical datasets

In addition to the primary broadband seismic and pressure data, several other geophysical datasets of value to the community were collected. Most OBS were equipped with one or more frame-mounted ocean water temperature and salinity sensors, separate from the APG temperature data streams. These temperature data are archived at IRIS DMC with channel codes RKO, and location codes describing instrument type (Table S2).

An array of 398 "nodal" seismographs was deployed for one month along the road system of Kodiak Island to provide opportunities for high-resolution investigation of structure and seismic activity associated with subduction. These three-component 5-Hz Fairfield Nodal Zland geophones (249 provided by IRIS-PASSCAL; 149 from University of Utah) were deployed along the road system on Kodiak Island (Figure 4) from mid-May to mid-June 2019, with the full 398 station array recording at 500 Hz for 25 days. Average station spacing along the ~60 km road system was ~200 m. The array extends approximately 50 km in the down-dip direction directly over the region that ruptured in the great M9.2 1964 earthquake. Demobilization of the nodes was done in concert with an undergraduate short course, held on Kodiak Island in June 2019.

Data from the nodal network is available under network code "8J" via the IRIS Data Center (dmc.iris.edu).

200

201

202

203

204

205

206

207

208

209

210

211

212

213

214

215

216

217

218

219

198

199

During the nodal array deployment, the R/V Marcus G. Langseth shot an airgun array into the eastern two-thirds of the AACSE footprint from June 7 to June 24, 2019 (cruise MGL1903). The objectives of this active source seismic experiment were to acquire a 3D wide-angle refraction dataset by providing acoustic sources to be recorded by the AACSE broadband (Figure 5) and nodal seismometer arrays, and to image shallow crustal structure (Figure 6) with reflections recorded by the R/V Langseth streamer. Acoustic pulses were generated by the 6600 cu.in tuned airgun array of the R/V Langseth, towed at a depth of 12m. Acoustic pulses were triggered every 400 m at a nominal pressure of ~1,950 psi. The shot spacing was kept fixed throughout the survey. The active source experiment consists of 12 profiles spaced every ~34 km along-trench and oriented sub-orthogonal to the trench axis, as well as shorter connecting profiles (Figure 5A). Trench-perpendicular profile lengths range between 150 and 275 km, and profiles extend ~60-120 km outboard of the trench onto the Pacific plate. Total active source profile length is 3146 km. For the first 1751 km (i.e. from profiles MC01 through MC07), a 4.05km-long, 324-channel streamer was towed at a 12 m depth to collect coincident multichannel seismic data. With a 400 m shot spacing, fold coverage (i.e. number of traces in each common midpoint) is 5. Despite this low fold coverage, multichannel seismic data are of very good quality in intermediate and deep water depths (Figure 6), but suffer from spatial aliasing in shallow water depths. Broadband station gathers are separately archived at the IRIS DMC as assembled dataset #19-026.

Additional underway data was collected on all cruises. Because the deep-water sea floor off Alaska is poorly mapped, additional cruise days were allocated for multibeam mapping by the R/V Langseth during the final recovery cruise. Mapping focused on the incoming plate in the region of outer-rise faulting (Masson, 1991; Shillington et al., 2015) and in the region of the complex M7.9 January 2018 offshore Kodiak earthquake (Ruppert et al., 2018). Seafloor bathymetry was recorded on the R/V Langseth using a Kongsberg EM122 Multibeam Echo Sounder, and with a higher-frequency (30 kHz vs 12 kHz) Kongsberg EM302 system on the R/V Sikuliaq. Concurrently, sub-bottom profiles were recorded on all cruises, using the Langseth's 3.5 kHz Knudsen 3260 chirp echosounder, or the Sikuliaq's Topas PS18 system. All underway data are available via the Marine Geoscience Data System (MGDS, marine-geo.org) as part of the AACSE data stream (Table S2). Example bathymetry and a sub-bottom profile from near the 2018 M7.9 Offshore Kodiak earthquake are shown in Figure 7.

3. Data Availability and Quality

Data collection began in May 2018 with the full onshore-offshore broadband seismic network installed by July 22, 2018. Broadband seismic data collection continued through September 2019, with instrument retrieval beginning August 11, 2019. AACSE stations recorded good quality seismic data, showing clear earthquake signals from local and teleseismic events on at least one component during 79% of the deployment, and data of any quality during 88% of the deployment (Table S1).

Of 30 land stations, five sites lost timing for a substantial portion of the experiment, from 34 to 285 days, but continued recording good quality data (Table S1). For these sites, it was possible to calculate approximate timing corrections using an ambient noise method (details in the Supplement) with timing correction accuracy of ~0.05 seconds; all but one of these time drift corrections are <1.0 second. Seven additional stations had short time periods (< 5 days) with good data but questionable timing quality, and two stations have longer periods (14-287 days) with both poor timing quality and unusable data (Table S1). Timing problems typically resulted from bear damage to GPS antennas and connecting cables. In total, land stations recorded good quality seismic data showing local and teleseismic earthquake signals on at least one component during ~90% of the deployment, and any quality data, including periods of instrumental noise, during ~93% of the deployment (Table S1). 370 of 398 nodal seismometers were operating upon retrieval, indicating a data recovery rate of ~93%. Additional details of nodal seismometer recovery rates are also included in the Supplement.

Of 75 OBS stations, 4 OBS were unrecoverable, and 3 OBS systems failed without recording seismic, pressure, or hydrophone data. For an additional 4 OBS, broadband seismometers did not record ground motion, though differential and absolute pressure gauges continued to record accurately for large portions of the experiment (Table S1) and may be an adequate substitute for some applications. A number of individual OBS instruments or channels also failed or exhibited notable noise; known problems are documented in Supplementary Table S1. For three LDEO OBS (LT02, LT08, LT11), the primary datalogger shut down before recovery, and no final GPS clock sync was possible. No clock-drift correction has been applied to data stored

at the IRIS DMC for these sites. However, we provide here approximate timing corrections using ambient noise cross correlation, described in the Supplement. For all three sites, cross correlation reveals clock drift of less than 1 second by the end of the experiment. Of the four unrecoverable OBS, three failed to re-establish acoustic communication, and therefore could not release from the seafloor. At the fourth unrecoverable OBS, a shielded shallow water site, the recovery line broke and became suspended in the water column, making recovery with the ROV Jason too dangerous to complete. Thirteen of the nineteen APG instruments successfully retrieved from the shallow water sites (documented in Table S1 and the Supplement) have uncertain timing due to failure of time synchronization between the seismometer datalogger and the APG datalogger, instead relying on a moderate-drift-rate clock internal to the APG datalogger. For these thirteen sites, uncertainty in APG timing is unknown (Supplement Section 5.3.2), but may be reduced by cross-correlation with collocated seismic vertical sensors.

In total, OBS recorded good quality seismic data showing local and teleseismic earthquake signals on at least one component during ~74% of the deployment, and any data, including periods of instrumental noise, during ~85% of the deployment (Table S1). Many of the LDEO OBS reached their recording capacity at ~451 days deployed, between 4 and 15 days before instrument recovery (Table S1). OBS data recovery rates partly reflect the extraordinary duration of the AACSE experiment: 15-16 month deployment for LDEO OBS, and 13-14 months for WHOI OBS. This long-duration experiment was enabled by a redesign of OBS battery packs to extend deployment duration (Abers et al., 2019). We note that the chances of instrumental failure increase with OBS deployment duration. Previous OBS deployments have only lasted ~12

months, meaning the AACSE experiment tested the limits of OBS engineering more than previous deployments. To our knowledge, AACSE represents the longest single U.S. OBS deployment to date.

To evaluate environmental noise within the AACSE network, we use IRIS's noise-pdf MUSTANG tool (Casey et al., 2018), which provides probability density functions of seismic noise for each site throughout the recording period. Figure 8 shows the median vertical and horizontal noise spectra as a function of instrument location and water depth, and Figure 9 shows median vertical noise across the network in a 3-8 Hz local earthquake band (Figure 9A) and a 20-40 second long-period band (Figure 9B). Both figures show data only from sites with good quality data recorded throughout the experiment.

The seismic noise environment varies significantly across the network (Figures 8, 9). On land, long-period noise on all channels is relatively lower (Fig 8A,B, dark blue and white curves), but short period noise can be substantially higher, particularly at sites along the Bering Sea coast of the Alaska Peninsula (Fig 8A,B, some white curves). Kodiak Island sites are quiet overall (dark blue curves Fig 8A,B; Fig 9). Offshore, seismic noise characteristics vary largely as a function of local water depth (Fig 8C,D). The shallowest OBS sites on the continental shelf (<263 m water depth, station codes LT##) were deployed with a metal shield to protect the instruments (Abers et al., 2019). These sites (light blue curves, Fig 8A,B; yellow curves Fig 8C,D) show the largest microseismic peak shifted slightly towards shorter periods on the vertical component (Fig 8C) because of ocean wave interaction in shallow water, and a large noise peak at 6-30 seconds on

vertical and horizontal channels that is related to ocean swell causing seafloor deformation. All other OBS were deployed at depths between 903 and 5316 m and were not shielded. The 6-30 second noise peak is largely absent on deeper OBS, though noise on all channels at the longest periods > ~30 seconds does scale with water depth and may reflect oceanic infragravity waves (Webb & Crawford, 1999). For all OBS in this dataset, greater overall microseism noise and a slight shift of microseism noise to shorter periods may impact local earthquake detection because of additional noise between 1 and 8Hz relative to land sites.

4. Summary and Outlook

AACSE is a major shoreline-crossing seismic data set collected across North America's most active subduction margin. The 75 broadband OBS, 30 broadband land sites, 398 nodes, and accelerometers, pressure gauges, hydrophones, and temperature and salinity sensors deployed simultaneously with the EarthScope TA will provide wide-ranging opportunities for researchers to investigate the nature of subduction zones and the earthquakes and volcanoes they produce. This community dataset is now openly available only a few months after data recovery, and this initial assessment suggests that the data are relatively complete and of high quality. Production of a local seismicity catalog is now underway as a joint effort between the AACSE PI team and the Alaska Earthquake Center at the University of Alaska, Fairbanks, to jump-start investigations that require earthquake arrival picks. Additional data products are also being developed from active source seismic and marine geophysical data streams that will complement passive source observations. Experience with other successful community experiments suggests that a large number of seismologists and marine geophysicists will make use of these data, many of whom

have not previously used shoreline-crossing data, and we anticipate the data being used in novel and unforeseen ways.

5. Data and Resources:

All broadband seismic and accelerometer data, absolute and differential pressure gauge data, hydrophone data, APG-recorded temperature data, and OBS frame-mounted temperature data is available from the IRIS Data Management Center (dmc.iris.edu) under the network code 'XO' (https://doi.org/10.7914/SN/XO_2018). Prior to early July, 2020, some methods of data download from the IRIS DMC would produce incorrect station locations, by up to several km. Searches that requested latitude, longitude, and elevation from the "Station" metadata were correct, but the same information requested from individual "Channel" metadata was incorrect for a number of OBS. This problem should be corrected by publication of this article, but users are advised to double check coordinates against the DMC or Table S1 here.

All nodal seismometer data is available from the IRIS Data Management Center (dmc.iris.edu) under the network code '8J' (https://doi.org/10.7914/SN/8J_2019). Active source shot gathers on broadband instruments are available from the IRIS DMC as Assembled Dataset #19-026, and multi-channel reflection data recorded on the R/V *Langseth* streamer are available from the Marine Geoscience Data System (http://www.marine-geo.org/tools/entry/MGL1903).

Bathymetry and sub-bottom profiler data are also archived by the Marine Geoscience Data System (marine-geo.org). These data are retrievable by expedition codes: OBS deployment

cruises SKQ201811S and SKQ201816S, active source shooting cruise MGL1903, and OBS recovery cruises SKQ201918S and MGL1907. Data archival is also summarized in Table S2.

This article includes Supplemental Material. Table S1 describes broadband seismometer station locations, data recovery dates and rates, known data issues, and additional data streams available. Table S2 lists all types of data available as part of the AACSE data stream, channel codes if relevant, and data archive locations. The Supplemental Materials document includes additional details about deployment of land stations and OBS, further details of the nodal network deployment and recovery, and a description of timing corrections undertaken for broadband land and OBS sites that lost GPS timing but otherwise recorded quality data. Tables S3-S5 contain timing corrections for the three land sites with substantial timing drift (KT06, KT09, EP23), and Tables S6-S8 contain the timing corrections for OBS sites with uncertain timing (LT02, LT08, LT11).

Some figures were created using the Generic Mapping Tools version 4.2.1 (Wessel and Smith, 1998). ObsPy version 1.1.0 (Krischer et al., 2015) was also used for data processing and figure creation.

Acknowledgments: The AACSE project was funded by NSF award OCE-1654568 to Cornell.

Instrumentation onshore was provided by the IRIS-PASSCAL Instrument Center. Offshore instrumentation was provided, upgraded, and deployed by the WHOI and LDEO OBS Instrument Pools, and recovered by the successor WHOI OBS Instrument Center. Assistance from the

USGS's Alaska Volcano Observatory was invaluable to deployment on the Alaska Peninsula. The support staff of the R/V *Sikuliaq* and R/V *Marcus G. Langseth* provided support offshore, and numerous agencies and landholders supported the project onshore. Bill Danforth and Dave Foster contributed substantively to planning, analysis and processing of the underway multibeam and sub-bottom profiler data collection. Paul Johnson, Joan Gomberg, and Susan Hautala organized the collection and archival of OBS-mounted temperature and salinity data. We thank our reviewers for their valuable suggestions to improve the manuscript. Finally, we thank student volunteers for assistance in the field with node deployment and recovery on Kodiak Island.

References

Abers, G. A., A. N. Adams, P. J. Haeussler, E. Roland, P. J. Shore, S. Y. Schwartz, A. F. Sheehan, D. J. Shillington, S. Webb, D. A. Wiens, et al. (2019). AACSE: The Alaska amphibious community seismic experiment, EOS Trans. AGU, Online publ. https://eos.org/project-updates/examining-alaskas-earthquakes-on-land-and-sea

Buurman, H., C. J. Nye, M. E. West, and C. Cameron (2014). Regional controls on volcano seismicity along the Aleutian arc, *Geochemistry Geophys. Geosystems* **15**, 1147–1163, doi: 10.1002/2013GC005101.

Casey, R., M. E. Templeton, G. Sharer, L. Keyson, B. R. Weertman, and T. Ahern (2018). Assuring the quality of IRIS Data with MUSTANG, *Seismol. Res. Lett.* **89**, no. 2A, 630–639, doi: 10.1785/0220170191.

394 Davies, J., L. Sykes, L. House, and K. Jacob (1981). Shumagin seismic gap, Alaska Peninsula: 395 History of great earthquakes, tectonic setting, and evidence for high seismic potential, J. 396 Geophys. Res. 86, no. B5, 3821-3855, doi: 10.1029/JB086iB05p03821. 397 Estabrook, C. H., K. H. Jacob, and L. R. Sykes. (1994). Body wave and surface wave analysis of 398 large and great earthquakes along the eastern Aleutian arc, 1923-1993: Implications for 399 future great events. J. Geophys. Res., 99, 11,643-11,662. 400 Johnson, J. M., and K. Satake (1997). Estimation of seismic moment and slip distribution of the 401 April 1, 1946, Aleutian tsunami earthquake. Journal of Geophysical Research-Solid Earth, 402 102(B6), 11765-11774. 403 Krischer, L., T. Megies, R. Barsch, M. Beyreuther, T. Lecocq, C. Caudron, and J. Wassermann 404 (2015). ObsPy: A bridge for seismology into the scientific Python ecosystem, Comput. Sci. 405 Discov. 8, doi: 10.1088/1749-4699/8/1/014003. 406 Li, S., and J. T. Freymueller (2018). Spatial variation of slip behavior beneath the Alaska 407 Peninsula along Alaska-Aleutian Subduction Zone. Geophysical Research Letters, 45(8), 408 3453-3460. 409 López, A. M., and E. A. Okal (2006). A seismological reassessment of the source of the 1946 410 Aleutian "tsunami" earthquake, Geophys. J. Int. 165, 835-849, doi: 10.1111/j.1365-411 246X.2006.02899.x.

- 412 Masson, D.G. (1991). Fault patterns at outer trench walls. *Mar Geophys Res* 13, 209–225.
- 413 https://doi.org/10.1007/BF00369150
- 414 Miller, T. P., and R. L.Smith (1987). Late Quaternary caldera-forming eruptions in the eastern
- 415 Aleutian arc, Alaska. Geology, 15(5), 434–438.
- 416 Peterson, J. (1993). Observations and modeling of seismic background noise, U.S. Geol. Surv.
- 417 Open-File Rept. 93-322, 94 pp.
- Ruppert, N. A., C. Rollins, A. Zhang, L. Meng, S. G. Holtkamp, M. E. West, and J. T. Freymueller
- 419 (2018). Complex faulting and triggered rupture during the 2018 Mw 7.9 offshore Kodiak,
- 420 Alaska, earthquake, *Geophys. Res. Lett.* 45, 7533–7541, doi: 10.1029/2018GL078931.
- 421 Shillington, D. J., A. Becel, M. R. Nedimovic, H. Kuehn, S. C. Webb, G. A. Abers, K. M. Keranen, J.
- 422 Li, M. Delescluse, and G. A. Mattei-Salicrup (2015). Link between plate fabric, hydration
- and subduction zone seismicity in Alaska, *Nat. Geosci.* 8, 961–964, doi: 10.1038/ngeo2586.
- Tape, C., D. C. Heath, M. G. Baker, S. Dalton, K. Aderhold, and M. E. West (2019). Bear
- 425 encounters with seismic stations in Alaska and northwestern Canada, Seismol. Res. Lett.
- 426 90, no. 5, 1950–1970, doi: 10.1785/0220190081.
- Toomey, D. R., R. M. Allen, A. H. Barclay, S. W. Bell, P. D. Bromirski, R. L. Carlson, X. Chen, J. A.
- 428 Collins, R. P. Dziak, B. Evers, et al. (2014). The Cascadia initiative: A sea change in
- seismological studies of subduction zones, *Oceanography* 27, no. 2, 138–150, doi:
- 430 10.5670/oceanog.2014.49.

431 von Huene, R., Miller, J. J., and W. Weinrebe. (2012). Subducting plate geology in three great 432 earthquake ruptures of the western Alaska margin, Kodiak to Unimak. Geosphere, 8(3), 433 628-644. 434 Webb, S. C., and W. C. Crawford, (1999). Long-period seafloor seismology and deformation 435 under ocean waves. Bull. Seismol. Soc. Amer., 89(6), 1535–1542. 436 Wessel, P., and W. H. F. Smith (1998). New, improved version of generic mapping tools 437 Released, Eos (Washington. DC). 79, no. 47, 579-579. 438 Witter, R. C., R. W. Briggs, S. E. Engelhart, G. Gelfenbaum, R. D. Koehler, and W. D. Barnhart 439 (2014). Little late Holocene strain accumulation and release on the Aleutian megathrust 440 below the Shumagin Islands, Alaska, Geophys. Res. Lett. 41, 2359–2367, doi: 10.1002/2014GL059393. 441

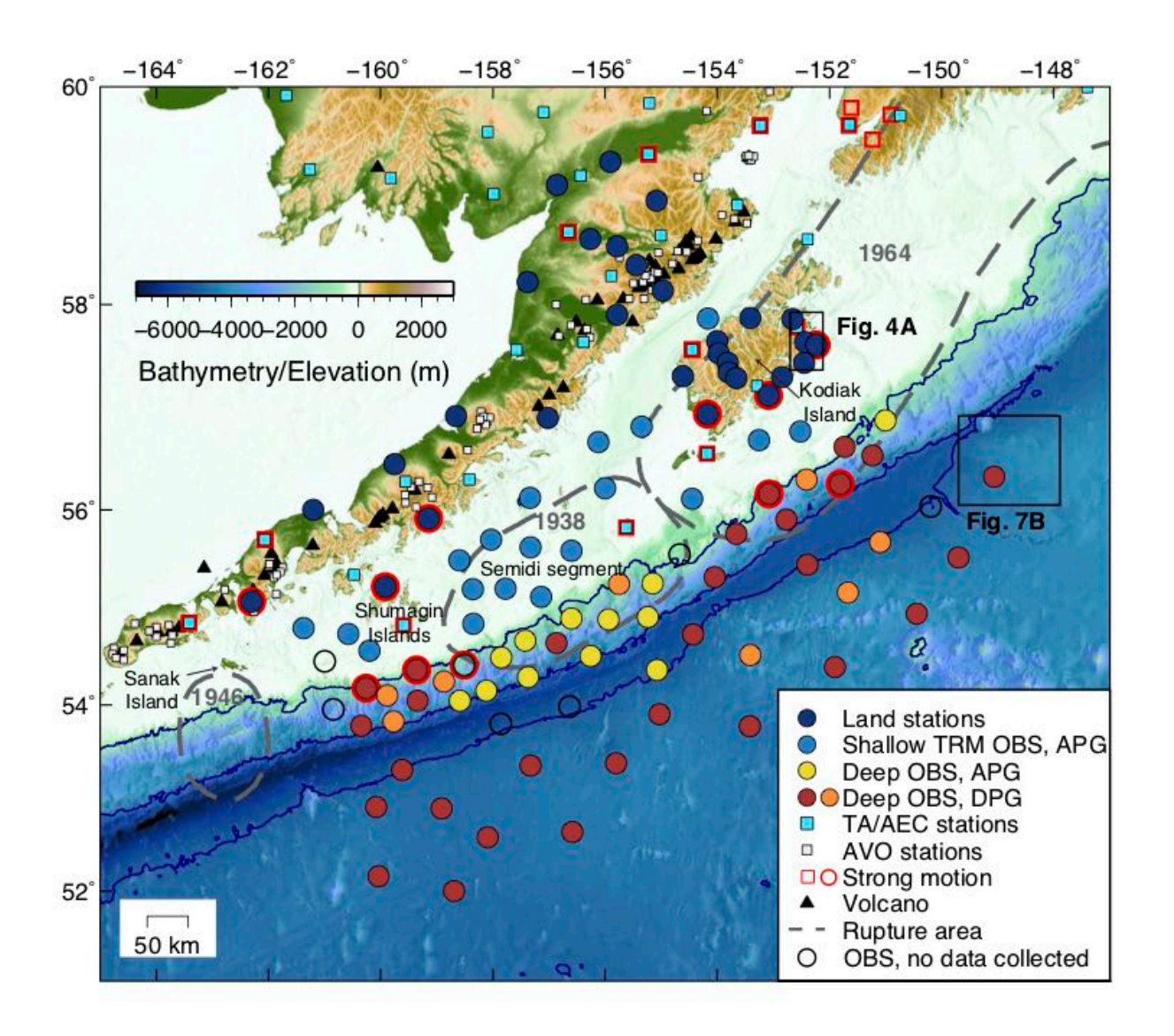


Figure 1. The Alaska Amphibious Community Seismic Experiment (AACSE) broadband array.

Symbols corresponding to different instrument types are shown in the legend. Gray dashed lines outline rupture areas of historical earthquakes (Davies et al., 1981). Black boxes indicate extents of Figures 4A and 7B. Dark blue lines are the 1000 and 5000 m oceanic depth contours. Empty circles indicate sites that were either not recoverable, or that failed soon after deployment and recorded little to no data of any kind. Note that some Alaska Volcano

Observatory (AVO) sites have only short-period instruments, but are shown for completeness.

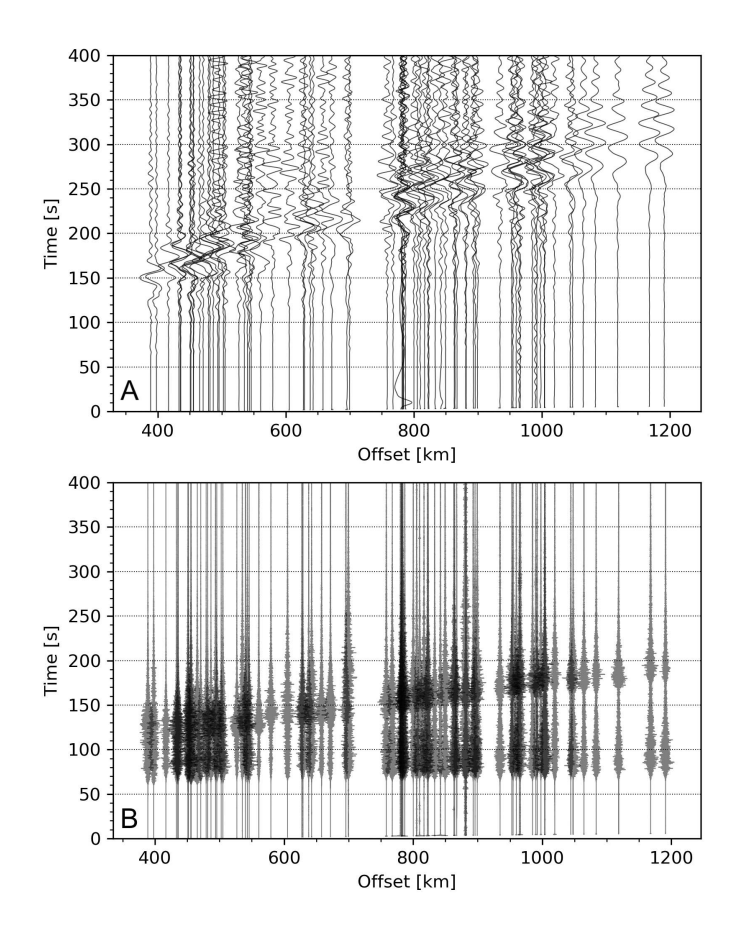


Figure 2. The Nov. 2018 M7.1 Anchorage earthquake recorded by the AACSE network. **A:**Bandpass filtered 10-100 seconds. **B:** Bandpass filtered 2-10 Hz. Data amplitudes in both panels are normalized within each trace.

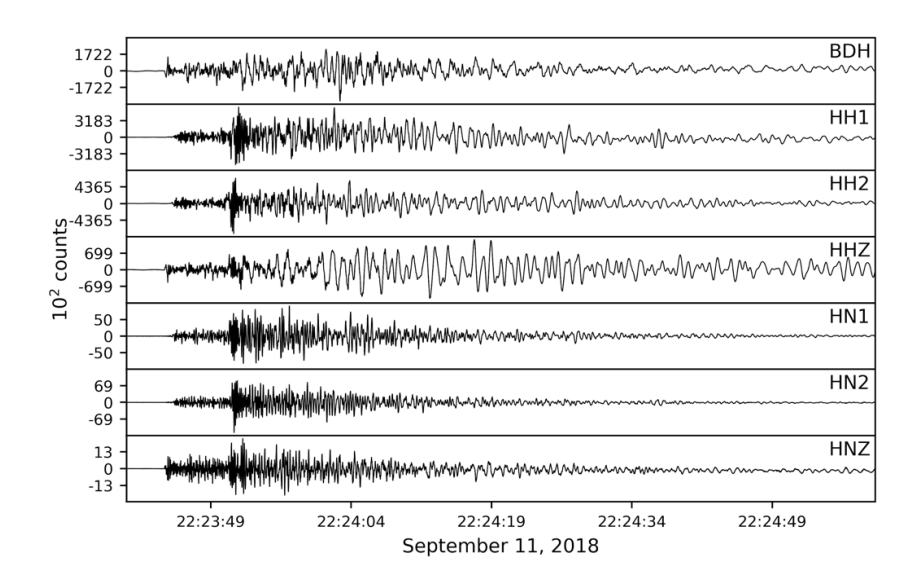


Figure 3. Example local earthquake recorded on all channels of OBS site WS71: Differential pressure gauge (BDH), broadband seismometer (HH*), and accelerometer (HN*). All channels are unfiltered. This M3.0 earthquake occurred Sept 11, 2018, 22:23:38 UTC, approximately 25 km from WS71.

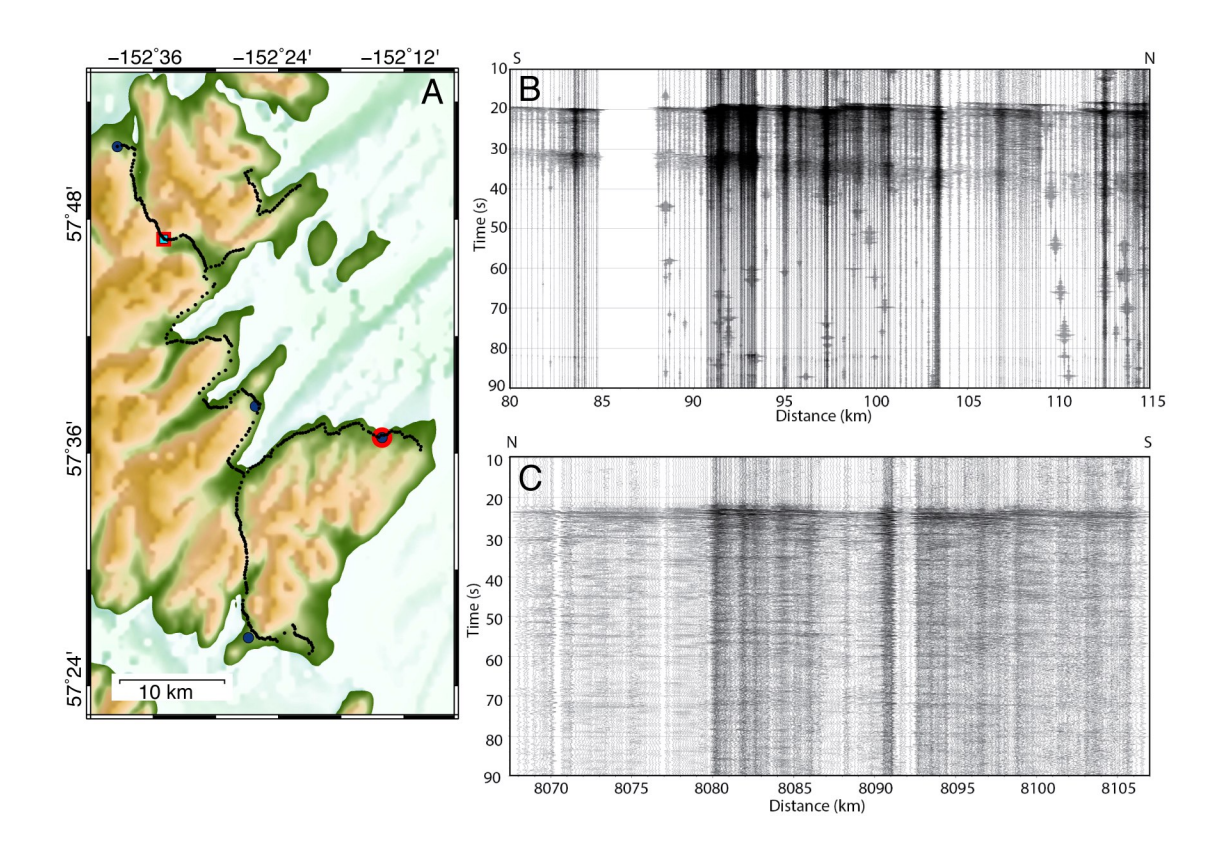


Figure 4. Kodiak Island nodal array and example recorded earthquakes. A. Nodal array network setup. The black dots show node locations along road systems on Kodiak Island, appearing to overlap in regions with high node density. The other symbols are the same as Figure 1. The location of panel A is also shown in Figure 1. B. Kodiak node array recording of a M3.1 local earthquake that occurred offshore northeast of Kodiak Island (58.2834, -151.3153) on June 7, 2019 (14:59:17.906 UTC). Data are bandpass filtered at 1-20 Hz, and amplitudes are normalized within each trace. C. Kodiak node array recording of M5.8 teleseismic event from Sichuan, China (28.4005, 104.9294) on June 17, 2019 (14:55:45.482 UTC). These data are bandpass filtered at 0.5-2 Hz, and amplitudes are normalized within each trace.

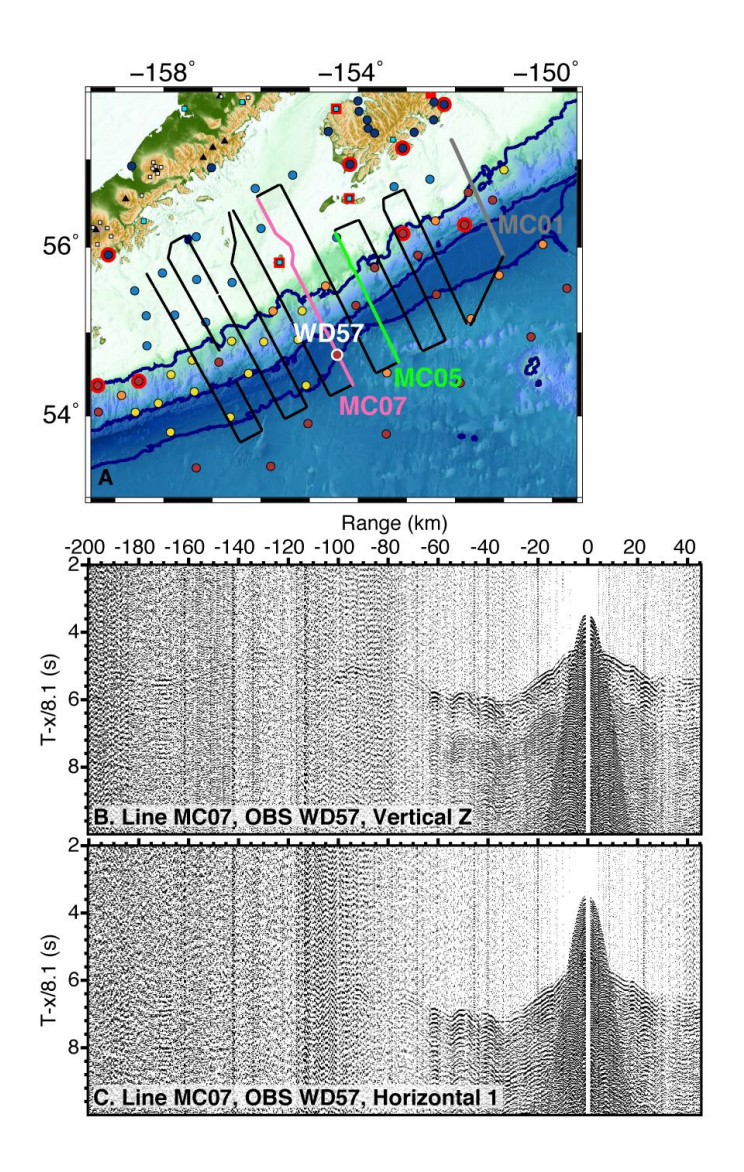
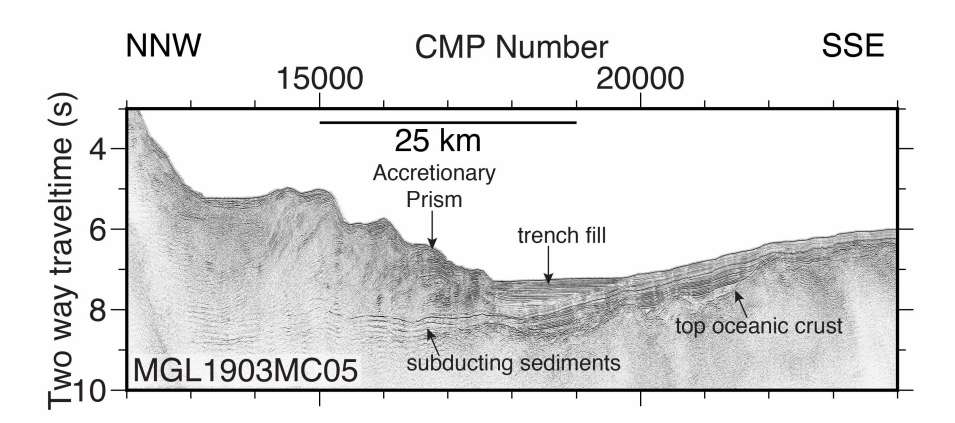


Figure 5: Example of active source OBS data. **A:** Map showing active source shot profiles in black, with profiles mentioned in the text highlighted. **B:** Vertical and **C:** one of the horizontal components of deep water OBS WD57 recording shots from profile MC07.



474 Figure 6: Example of onboard processed multichannel seismic data showing a short section of
 475 profile MC05 (Figure 5) highlighting near-trench structures.

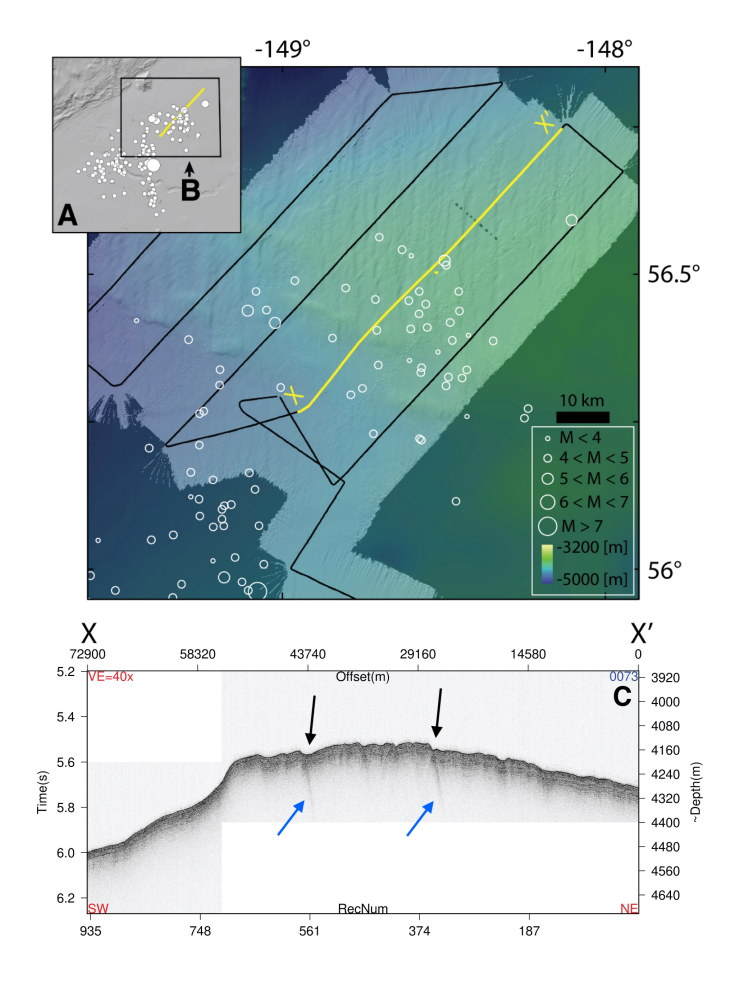


Figure 7. High resolution multibeam bathymetry and co-located sub-bottom profile over the northeastern extent of the 2018 M7.9 offshore-Kodiak earthquake rupture zone and aftershock area (Ruppert et al., 2018). A. Aftershock sequence of the M7.9 event, outboard of the Alaska-Aleutian trench. Seismicity from 3 weeks before and after the main shock are shown as white dots, sized by magnitude (Earthquake locations from USGS COMCAT catalog (https://earthquake.usgs.gov/earthquakes/search/, last accessed 13 April, 2020). B. Seafloor bathymetry collected by the R/V Langseth during the final AACSE OBS recovery leg, revealing north-south oriented lineaments within the aftershock area. Black lines are ship tracks, and white circles are the same earthquakes shown in panel A. C. Sub-bottom profile from the X-X' transect indicated by the yellow line in panels A and B. Approximate depth conversions and

vertical exaggeration assume a constant time to depth conversion of 1500 m/s P-wave velocity.

The locations of dipping features (blue arrows) and folded sediments (black arrows) correspond with two north-south bathymetric lineaments shown in B.



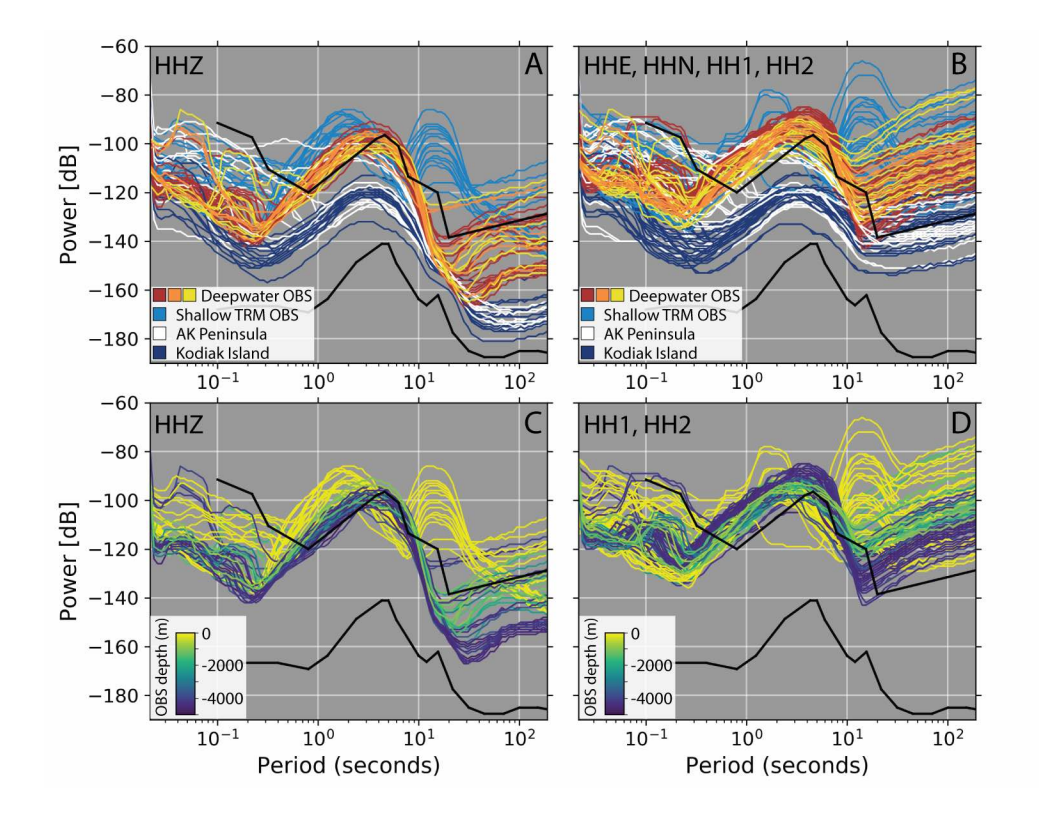


Figure 8: Median noise spectra of the AACSE network. A-B: Median noise spectra on vertical (A) and horizontal (B) channels of all AACSE sites, colored by region of the network. Colors match Figure 1, except for Alaska Peninsula sites, which are white here. C-D: Median noise spectra on vertical (C) and horizontal (D) channels of OBS sites, colored by water depth. All: Data plotted are median noise spectra at each site for the duration of the experiment. Sites with excessive instrumental noise or data quality issues are removed. Thick black lines are the high and low noise reference models of Peterson (1993).

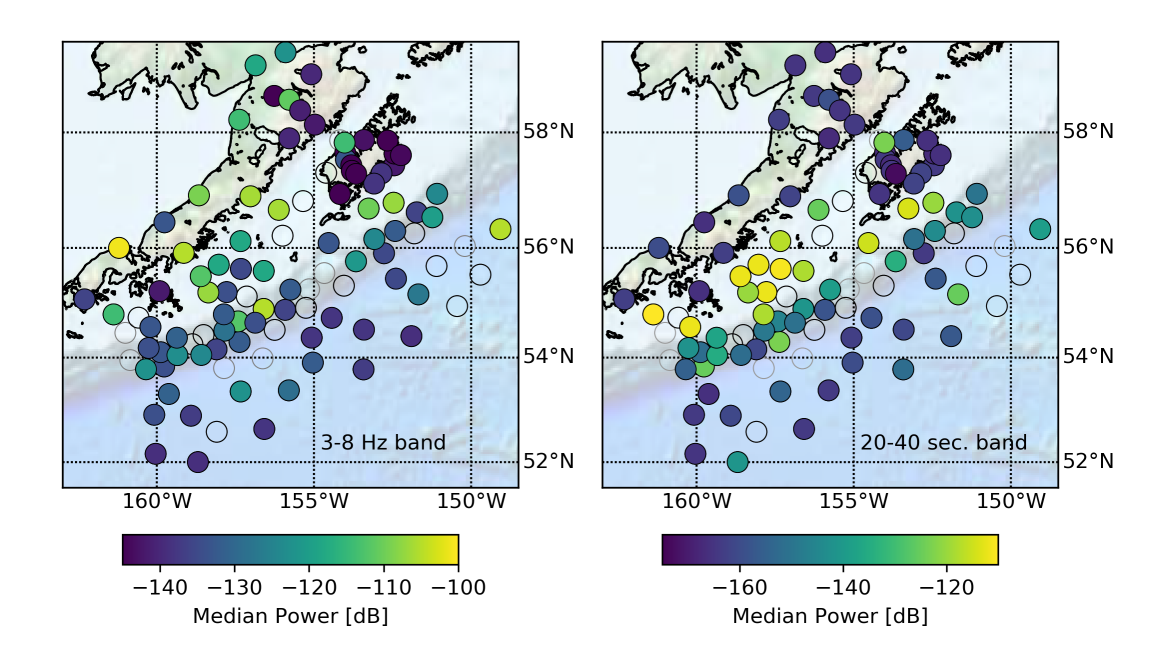


Figure 9: Median noise on the vertical channel across the AACSE broadband seismic network in a 3-8 Hz band (**left**) and a 20-40 second band (**right**). Data are calculated at each site for the duration of the experiment. Sites with little to no data retrieval are shown as empty grey circles, and sites with excessive instrumental noise or data quality issues are shown as empty black circles.

506 Author Affiliations and Mailing Addresses:

- Grace Barcheck^{1*}, Geoffrey A. Abers¹, Aubreya N. Adams², Anne Bécel³, John Collins⁴, James B.
- Gaherty⁵, Peter J. Haeussler⁶, Zongshan Li⁷, Ginevra Moore⁸, Evans Onyango⁹, Emily Roland⁸,
- Daniel E. Sampson¹⁰, Susan Y. Schwartz¹⁰, Anne F. Sheehan¹¹, Donna J. Shillington⁵, Patrick J.
- 510 Shore⁷, Spahr Webb³, Douglas A. Wiens⁷, Lindsay L. Worthington⁹

- ¹ Department of Earth and Atmospheric Sciences, Cornell University, 112 Hollister Drive, Ithaca,
- 513 NY, 14853-1504, USA.
- ² Department of Geology, Colgate University, 13 Oak Drive, Hamilton, NY, 13346, USA.
- 515 ³ Lamont-Doherty Earth Observatory, Columbia University, P.O. Box 1000, 61 Route 9W,
- 516 Palisades, NY 10964
- ⁴ Department of Geology and Geophysics, Woods Hole Oceanographic Institution, Mail Stop:
- 518 24, 266 Woods Hole Rd., Woods Hole, MA, 02543-1050, USA
- ⁵ School of Earth and Sustainability, Northern Arizona University, Room A108 Building 11,
- 520 Ashurst, 624 S Knoles Dr., Flagstaff, AZ, 86011, USA
- ⁶ U.S. Geological Survey, 4210 University Dr., Anchorage, AK, 99508, USA
- ⁷ Department of Earth and Planetary Sciences, Washington University in St. Louis, Campus Box
- 523 1169, 1 Brookings Dr., St. Louis, MO, 63130-4899, USA
- ⁸ School of Oceanography, University of Washington, 1503 NE Boat St., Box 357940, Seattle,
- 525 WA, WA 98195-7940, USA
- 526 ⁹ Department of Earth and Planetary Sciences, University of New Mexico, 1 University Place,
- 527 Albuquerque, NM, 87131-0001, USA

528	¹⁰ Department of Earth and Planetary Sciences, University of California Santa Cruz, 1156 High
529	Street, Santa Cruz, CA 95064
530	¹¹ Cooperative Institute for Research in Environmental Sciences and Department of Geologica
531	Sciences, University of Colorado, Boulder, Colorado 80309, USA